This article was downloaded by: [Observatoire de Paris - Bibliothèque]
On: 09 July 2012, At: 02:42
Publisher: Taylor & Francis
Informa Ltd Registered in England and Wales Registered Number: 1072954 Registered office: Mortimer House, 37-41 Mortimer Street, London W1T 3JH, UK

Geophysical & Astrophysical Fluid Dynamics

Publication details, including instructions for authors and subscription information:
http://www.tandfonline.com/loi/ggaf20

Two-dimensional non-linear simulations of the magnetostrophic magnetorotational instability

Ludovic Petitdemange [a]

[a] Laboratoire de Radioastronomie, Ecole Normale Supérieure, Paris, France

Version of record first published: 30 Mar 2010

To cite this article: Ludovic Petitdemange (2010): Two-dimensional non-linear simulations of the magnetostrophic magnetorotational instability, Geophysical & Astrophysical Fluid Dynamics, 104:2-3, 287-299

To link to this article: http://dx.doi.org/10.1080/03091921003636496

PLEASE SCROLL DOWN FOR ARTICLE

Full terms and conditions of use: http://www.tandfonline.com/page/terms-and-conditions

This article may be used for research, teaching, and private study purposes. Any substantial or systematic reproduction, redistribution, reselling, loan, sub-licensing, systematic supply, or distribution in any form to anyone is expressly forbidden.

The publisher does not give any warranty express or implied or make any representation that the contents will be complete or accurate or up to date. The accuracy of any instructions, formulae, and drug doses should be independently verified with primary sources. The publisher shall not be liable for any loss, actions, claims, proceedings, demand, or costs or damages whatsoever or howsoever caused arising directly or indirectly in connection with or arising out of the use of this material.

Geophysical and Astrophysical Fluid Dynamics
Vol. 104, Nos. 2–3, April–June 2010, 287–299

Taylor & Francis
Taylor & Francis Group

Two-dimensional non-linear simulations of the magnetostrophic magnetorotational instability

LUDOVIC PETITDEMANGE*

Laboratoire de Radioastronomie, Ecole Normale Supérieure, Paris, France

(*Received 12 June 2009; in final form 27 November 2009*)

We have shown that a simple, modified version of the Magnetorotational Instability (MRI) can, in principle, develop in the Earth's outer liquid core in the presence of a background shear (see Petitdemange, Dormy and Balbus, MagnetoStrophic MRI in the Earth's outer core. *Geophys. Res. Lett*. 2008, **35** 15305). We refer to this instability as the Magnetostrophic MRI (MS-MRI). In this article, we extend our investigations to the nonlinear regime and present results from global axisymmetric simulations in spherical geometry. We show that as the angular momentum is transported outward, the MS-MRI saturates by rapidly changing the initial shear profile. Therefore, the saturation process differs substantially from traditional MRI applications (e.g. accretion disks) in which the background shear is essentially fixed. We show that the MS-MRI appears as a new constraint which limits the maximum differential rotation. To illustrate this mechanism, we apply this work to a Jupiter-like planet, and argue that the magnetic field eventually destabilises the conducting zone of this planet. According to these results, purely hydrodynamic models for the deep origin of the banded structure of Jupiter may need to be modified.

Keywords: MHD instability; MRI; Planetary interiors; Saturation

Downloaded by [Observatoire de Paris - Bibliothèque] at 02:42 09 July 2012

1. Introduction

The Magnetorotational Instability (MRI) is known to trigger the turbulence in sufficiently ionised accretion disks. The instability was first noted by Velikhov (1959) and Chandrasekhar (1961). Then, Balbus and Hawley (1991) understood its importance for astrophysics (see Balbus and Hawley (1998) for a useful review). Later, it was also confirmed numerically by Hawley *et al*. (1995, 1996; henceforth HGB), Brandenburg *et al*. (1995) and Matsumoto *et al*. (1996). Application of the MRI to planetary interiors has been introduced by Petitdemange *et al*. (2008; henceforth PDB08). In this context, the following differences compared to traditional accretion disk simulations occur: first, differential rotation is much weaker than in accretion disks; second, the shear profile can change in time whereas it is assumed to be fixed in Keplerian disks in which the shear is imposed by the gravitational potential of the massive central object and third, planetary interiors are known to be strongly affected by magnetic resistivity.

*Email: ludovic.petitdemange@lra.ens.fr

Geophysical and Astrophysical Fluid Dynamics
ISSN 0309-1929 print/ISSN 1029-0419 online © 2010 Taylor & Francis
DOI: 10.1080/03091921003636496

Downloaded by [Observatoire de Paris - Bibliothèque] at 02:42 09 July 2012

Planets are in rapid rotation and the Coriolis force strongly affects their interior dynamics (Proudman 1956). Consequently, these systems can be studied in the magnetostrophic (MS) regime. PDB08 performed a linear stability analysis of shear layers in rapidly rotating spherical shells affected by a vertical magnetic field. This model was designed to be very simple, with no thermodynamics. However, there was a shear profile driven by an imposed super-rotation of the inner core. With the WKB method and direct numerical simulations, PDB08 showed that a slightly modified version of the MRI, the so-called Magnetostrophic MRI (MS-MRI) can take place for the parameter regime relevant to the Earth's outer core. The growth time of this instability is directly proportional to the differential rotation.

In this article, we consider the same model as PDB08. It is assumed that convective motions induce a zonal shear, which in turn allows the development of the MS-MRI. Here, we focus on the nonlinear saturation of the MS-MRI in order to better understand its physical significance. In particular, we show by means of direct numerical simulations using the PARODY code (Dormy *et al.* 1998 and later collaborative developments) that saturation is a consequence of modifications in the rotation profile. When nonlinearities start to play an important role, the angular velocity becomes constant on cylinders. The rate of shear decreases with time until it reaches a limit which depends on the dimensionless parameters applied.

The plan of this article is as follows. In section 2, we explore the nonlinear evolution of the MS-MRI as it occurs in the Spherical Couette Flow. In section 3, we remove the inner core effects and apply a background velocity field $U_0(s)\mathbf{e}_\phi$. In section 3.1, we present the method and list all parameters. In section 3.2 we investigate the first stage of the saturation phase. Section 3.3 is devoted to the final saturated state, from which we propose the existence of a maximal shear allowed by the MS-MRI. In section 4, we present a tentative application to the banded structure of Jupiter, and we conclude in section 5.

2. Nonlinear evolution of the MS-MRI occurring in the spherical Couette flow

2.1. *Equations*

As an initial velocity field, we consider the linear steady MHD solution of the Spherical Couette Flow problem. Let the rotation rate of the inner sphere of radius $r_i = 0.35 r_o$ be denoted by Ω_i and that of the outer sphere by Ω_0 with $(\Omega_i - \Omega_0)/\Omega_0 \ll 1$ (see also PDB08). A purely vertical and uniform magnetic field $\mathbf{B}_0$ is imposed and Ω_i and Ω_0 are kept fixed during the simulation. For the subsequent evolution of our initial velocity field, we solve the full nonlinear MHD equations

$$\frac{\partial \mathbf{u}}{\partial t} + \mathbf{u}\cdot\nabla\mathbf{u} = E\nabla^2\mathbf{u} - 2\mathbf{e}_z\times\mathbf{u} - \nabla\pi + \frac{\Lambda E}{P_m}(\nabla\times\mathbf{b})\times(\mathbf{B}_0+\mathbf{b}), \tag{1}$$

$$\frac{\partial \mathbf{b}}{\partial t} = \frac{E}{P_m}\nabla^2\mathbf{b} + \nabla\times[\mathbf{u}\times(\mathbf{b}+\mathbf{B}_0)], \tag{2}$$

$$\nabla\cdot\mathbf{b} = 0, \quad \nabla\cdot\mathbf{u} = 0, \tag{3}$$

in which we have introduced the dimensionless parameters

$$E = \frac{\nu}{\Omega_0 r_o^2}, \quad \Lambda = \frac{B_0^2}{\rho\mu\eta\Omega_0} \quad \text{and} \quad P_m = \frac{\nu}{\eta}, \tag{4}$$

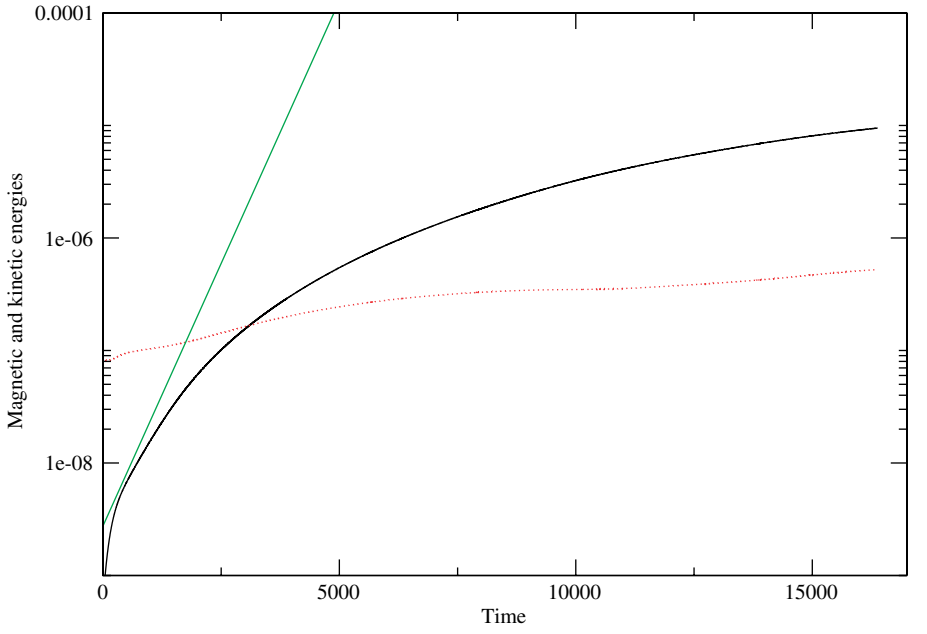

Figure 1. Nonlinear evolution of the kinetic and magnetic energies with time. The straight line represents the growth rate associated with the linear phase, it is given here as a reference. Its slope was obtained by solving the linearised MHD equations, as described in PDB08. The solid curve is the magnetic energy and the dashed curve is the total kinetic energy (i.e. in which the energy of the initial velocity field is included). The controlling parameters are $E = 10^{-6}$, $(\Omega_i - \Omega_0)/\Omega_0 = 0.005$, $P_m = 0.5$ and $\Lambda = 1$.

namely the Ekman number, the Elsasser number and the magnetic Prandtl number, respectively. Here, r_o is the radius of the outer sphere used as a fundamental length scale and time is scaled by $\tau_\Omega = 1/\Omega_0$ with Ω_0 being the global rotation rate of the system; B_0 is the characteristic scale for the magnetic field and is set to $|\mathbf{B}_0|$; ν, η, μ and ρ are the viscosity, the magnetic diffusivity, the permeability and the constant density of the fluid, respectively. The conductivities for the solid inner core and the fluid are the same, whereas the outer sphere is assumed to be insulating. We apply no-slip mechanical boundary conditions.

2.2. *Results*

In this article, we present results for one example with $E = 10^{-6}$, $P_m = 0.5$, $\Lambda = 1$ and $(\Omega_i - \Omega_0)/\Omega_0$. We define the growth rate as $\sigma(t) = (\mathrm{d}b^2/\mathrm{d}t)/b^2$, where $b^2 = |\mathbf{b}|^2$. Note that σ depends here on time, as we consider nonlinear problems. We find that the MS-MRI develops linearly at the beginning of the simulation, as predicted by PDB08. But, later on, the growth rate decreases with time (figure 1) because differential rotation is diminished by nonlinear effects. Hence the growth rate also decreases and is approximately proportional to differential rotation as already predicted by linear theory. Nevertheless, the induced magnetic energy can be amplified by the instability by several orders of magnitude compared to its initial value. The full spherical non-linear simulations did not reveal any unexpected behaviour, and produced a saturation

Downloaded by [Observatoire de Paris - Bibliothèque] at 02:42 09 July 2012

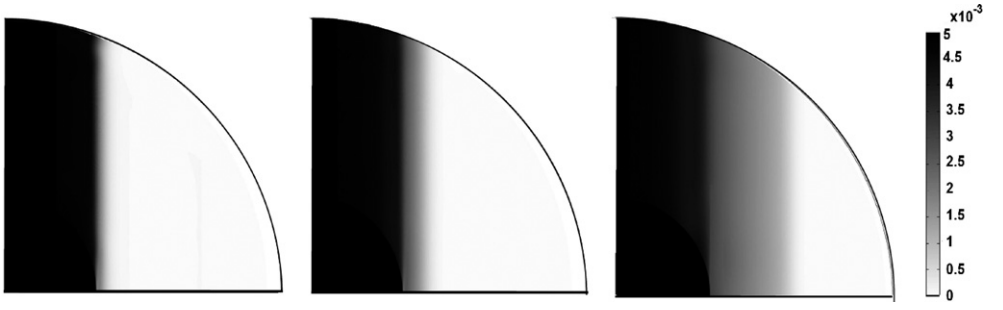

Figure 2. Evolution of the angular velocity changed by the nonlinear MS-MRI. From the left to right, the time corresponds to $t=0$, $t=2000$ and $t=5000$. The initial shear layer is progressively smoothed out. The parameters are the same as in figure 1.

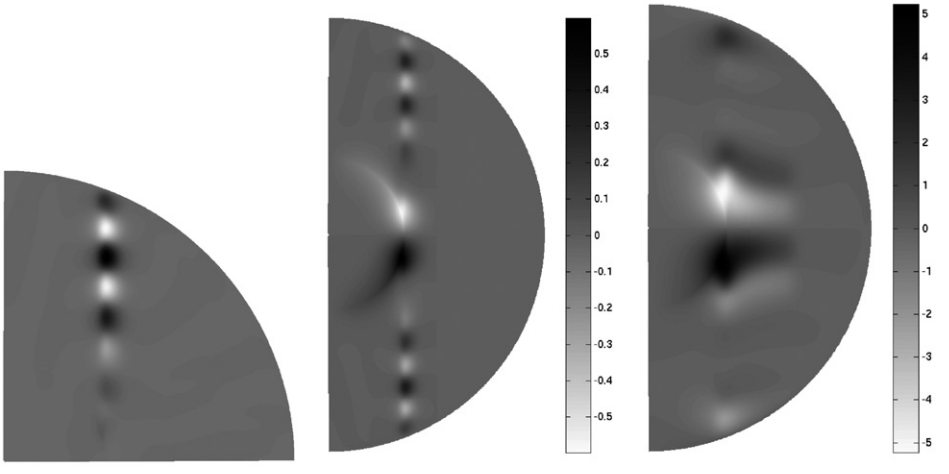

Figure 3. Evolution of the induced azimuthal magnetic field. As a reference, on the left, we present a result from a linear simulation (PDB08). The time corresponds to $t=2000$ (on the centre) and $t=5000$ (on the right). For this simulation, the parameters are $E=10^{-6}$, $P_m=0.5$, $(\Omega_i-\Omega_0)/\Omega_0=0.005$ and $\Lambda=1$.

Downloaded by [Observatoire de Paris - Bibliothèque] at 02:42 09 July 2012

mechanism comparable to the one described by the local study (through a modification of the shear).

Let us focus on the onset of the nonlinear effects. The differential rotation is caused by a moderate super-rotation of the inner sphere. The effect of the nonlinear terms is to slow down the flow inside the tangent cylinder, whereas, the rest of the flow is accelerated (figure 2). But, the rotation rate of the inner core is kept fixed causing a vertical shear close to the inner boundary, which distorts the applied vertical magnetic field. This effect gives rise to a dominant toroidal magnetic field (figure 3). This process develops rapidly, as soon as the nonlinearities become important. In addition, the radial shear which was initially regularly distributed along the tangent cylinder now decreases less rapidly near the inner sphere. As a result, the growth rate near the equatorial plane becomes stronger than in the rest of the fluid (figure 4).

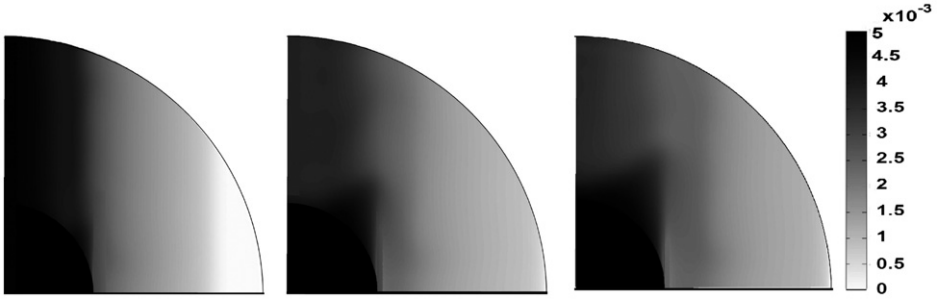

Figure 4. Evolution of the angular velocity changed by the nonlinear MS-MRI. From left to right, the time corresponds to $t = 7000$, $t = 14{,}000$ and $t = 17{,}000$. The initial shear layer is progressively smoothed out. The dimensionless parameters are the same as in figure 3.

Downloaded by [Observatoire de Paris - Bibliothèque] at 02:42 09 July 2012

After the linear phase, the growth of the MS-MRI mode reduces. As a result, the fluid inside the tangent cylinder can re-accelerate through the action of the Lorentz force. This is the reason why the vertical shear progressively moves away from the inner sphere towards the poles (figure 4). A global toroidal magnetic field, negative in the northern hemisphere and positive in the southern hemisphere, is induced. Consequently, when the stationary state is reached, only a very smooth radial shear is present, i.e. the angular velocity decreases almost linearly from the tangent cylinder to the outer sphere. Furthermore, the flow is strongly geostrophic (figure 5). The magnetic field is stretched in the cylindrical radial direction. The instability expands until it occupies the entire sphere (figure 4).

The results presented in this section strongly depend on the imposed super-rotation of the inner core. In order to analyse the instability in a simpler (and probably more generic) set-up, we suppress the effects of the inner core in the following sections by considering an imposed velocity field instead.

3. Modification of the shear profile

3.1. *Method*

The size of the inner sphere r_i is reduced so that it does not influence the instability. We again consider the nonlinear MHD equations presented in the previous section, but now with an additional velocity component $\mathbf{U}_0$ entering in the inertia term and the induction equation. The velocity field $\mathbf{u}$ is replaced with $\mathbf{U}_0 + \mathbf{u}'$ and we solve numerically the MHD equations for $\mathbf{u}'$. The applied velocity field $\mathbf{U}_0$ is defined as

$$\mathbf{U}_0(s) = A \exp\left[-\frac{(s-0.5)^2}{0.015}\right]\mathbf{e}_\phi. \tag{5}$$

Maintaining this flow, $\mathbf{U}_0$, for all time (but allowing for the full nonlinear development of $\mathbf{u}$) is physically equivalent to applying a distributed body force in the fluid, which drives the flow $\mathbf{U}_0$ through the Stokes balance.

The parameter A controls the magnitude of the applied flow. Such an imposed flow has several advantages compared to the configuration studied in the previous section. There, the shear caused by the super-rotating core varies sharply in a localised Stewartson layer

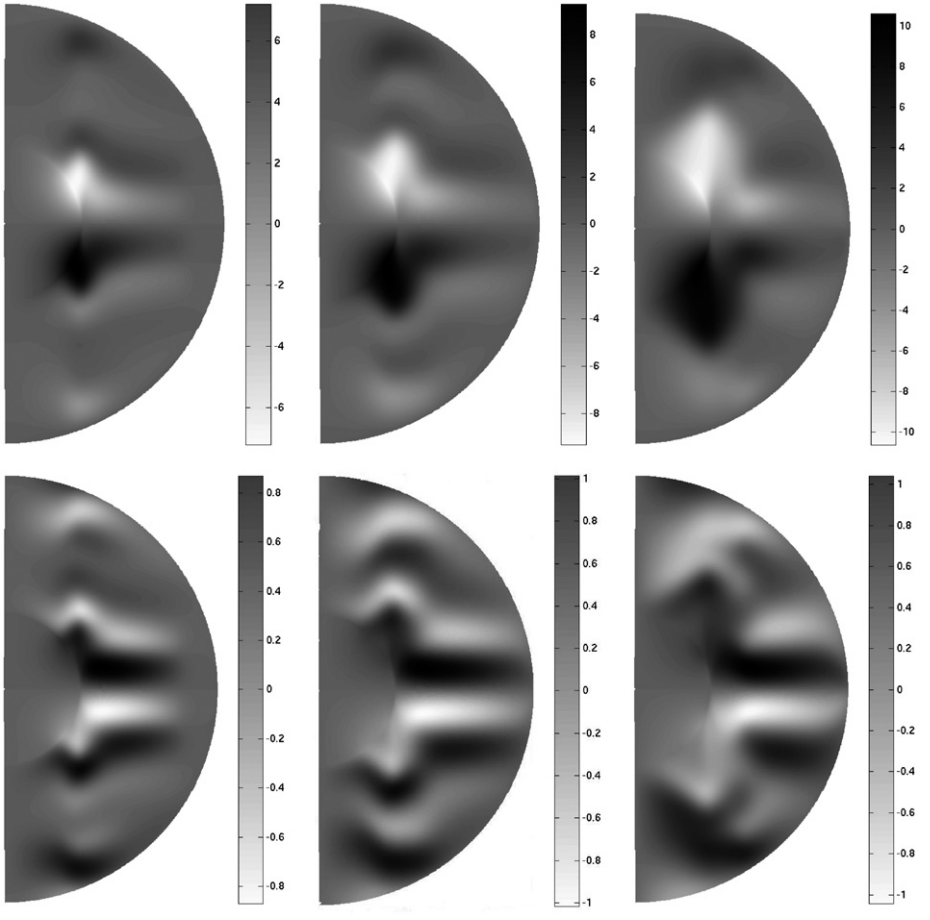

Figure 5. Meridional cuts of azimuthal b_ϕ (on the top) and radial b_s (on the bottom) at $t = 7000$, $t = 10{,}000$ and $t = 15{,}000$ (from left to right). The parameters are the same as in figure 3.

(Stewartson 1996). The width of the main layer depends on the Ekman number as $E^{1/4}$, which constrains the radial wave number to be very large. For the case of an applied field, having a flow with a comparable shear rate over larger distances is favourable for a numerical study, because the instability exhibits larger growth rates under these conditions. In addition, with a velocity profile as given in equation (5), the nonlinear terms can compensate the imposed velocity field $\mathbf{U}_0$. This leads to the saturation of the MS-MRI. Because of its smaller size, the inner core does not affect the solution, in contrast to the previous configuration. We locally measure the rate of shear by

$$R_o = \frac{1}{2}\left|\frac{\mathrm{d}(\ln \Omega)}{\mathrm{d}(\ln s)}\right| \quad \text{with} \quad \Omega = \frac{U_0 + u_\phi}{s}. \tag{6}$$

The resulting number, measuring the shear rate, monotonically decreases as soon as the instability starts to saturate. Far from the initial saturation phase, R_o still decreases until a final value which depends on the dimensionless parameters. The results presented in this article are obtained considering no-slip mechanical boundary

Downloaded by [Observatoire de Paris - Bibliothèque] at 02:42 09 July 2012

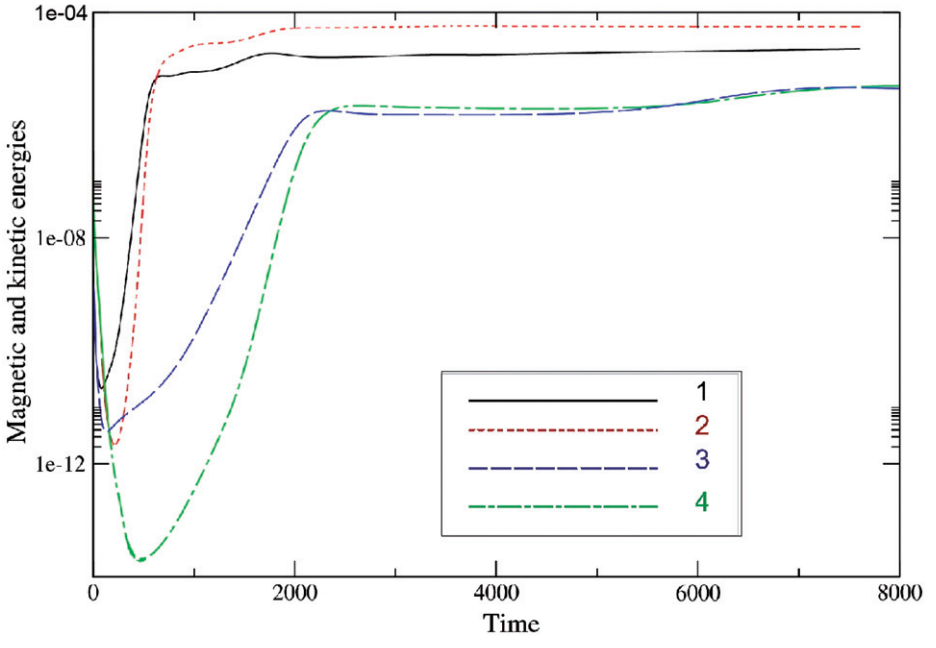

Figure 6. Nonlinear evolution of the kinetic (1, 4) and magnetic (2, 3) energies for two different parameters A, $A=0.03$ and $A=0.01$. The applied velocity field is that of equation 5 and the imposed magnetic field is purely vertical and uniform. The parameters for this simulation are $E=10^{-5}$, $P_m=0.5$ and $\Lambda=1$.

conditions on the outer sphere. But, in addition, we have performed numerical nonlinear simulations with stress-free conditions and we did not find any qualitative differences with the mechanism presented here. Using different boundary conditions confirmed our results.

3.2. *Saturation phase of the most unstable global mode*

Figure 6 shows the evolution of kinetic and magnetic energies for $A=0.03$ and $A=0.01$. The linear phase is in agreement with PDB08. Increasing the differential rotation causes k_z modes to vary on smaller scales (see equation (26) of PDB08). The energies of the perturbed fields increase by several orders of magnitude. The final energy levels depend directly on A, because the shear is the energy source of the MS-MRI.

The saturation process of the most unstable mode occurs by quickly reducing the differential rotation. The nonlinear effects make the angular velocity perturbations z-independent (figure 7), whereas the induced magnetic fields are just stretched radially (figure 8). The z-independence is already reached when the perturbations are still much smaller than the applied fields. As a result, the total vertical shear $\partial\Omega/\partial z$ is never comparable to the radial one expressed by R_o. When saturation occurs, the flow is constant on cylinders, while the induced magnetic field keeps the same vertical structure as in the linear phase.

Downloaded by [Observatoire de Paris - Bibliothèque] at 02:42 09 July 2012

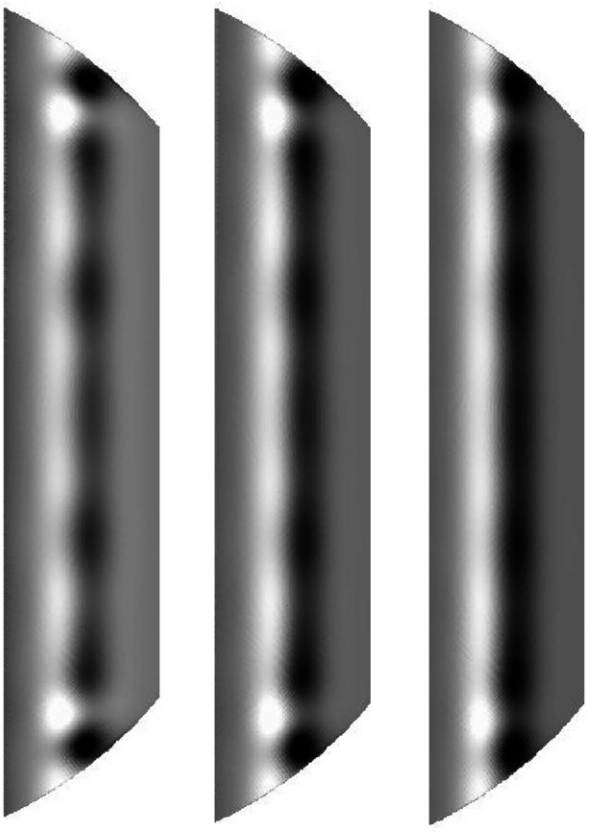

Figure 7. Illustration of the saturation mechanism. These meridional cross-sections show the angular velocity perturbations u_ϕ/s at time $t=400$ (on the left), $t=450$ (on the centre) and $t=500$ (on the right). Progressively, the nonlinearities yield a geostrophic angular velocity profile. The parameters used for this simulation are $E=10^{-5}$, $\Lambda=1$, $P_m=0.5$ and $A=0.03$.

3.3. *Long-term evolution*

While the new angular velocity profile is stable for the initial vertical wave number, it is unstable for modes with higher wave numbers. This secondary instability needs some time to develop, this is why figure 9 exhibits some plateaus. The temporal evolution of the maximum shear rate depends on the parameters as demonstrated in figure 9, where the influence of P_m is identified for fixed E, Λ and A parameters. This process goes on until the final state is reached which is a mode with approximately $k_z=\pi/0.8$ (figure 10).

For $E=10^{-5}$, the saturated state is obtained after a period ranging between $t=10{,}000$ and $t=15{,}000$, and for $E=10^{-6}$, it is reached after $t=25{,}000$. (The units of time are $1/\Omega_0$.) These time scales are very short compared to the magnetic diffusion time P_m/E and the viscous time E^{-1}. According to the above argument, the maximum differential rotation allowed by the system would correspond to a marginally stable state. Following the dispersion relation given in PDB08 with $\sigma=0$, we find

$$-4\frac{E\Lambda}{P_m}k_z^2 R_{o_{th}}+\left(\frac{E\Lambda}{P_m}\right)^2 k^2 k_z^2+4\frac{E^2}{P_m^2}k^4=0, \tag{7}$$

Downloaded by [Observatoire de Paris - Bibliothèque] at 02:42 09 July 2012

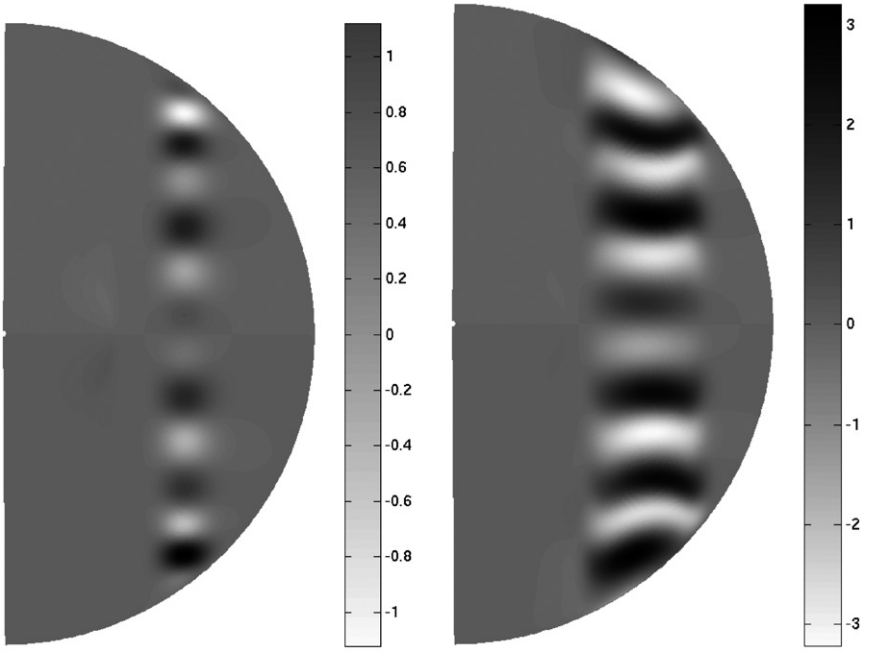

Figure 8. Meridional cross-sections of the azimuthal magnetic field for an applied banded structure with $A=0.03$ (at times $t=400$ on the left and $t=600$ on the right). These results are obtained numerically with an applied vertical magnetic field. The other parameters for this simulation are $E=10^{-5}$, $P_m=0.5$ and $\Lambda=1$.

with $k^2=k_s^2+k_z^2$ and where the critical Rossby number given by this theory $R_{o_{th}}$ is defined by the above equation. In order to calculate $R_{o_{th}}$ in table 1, we used $k_s=\pi/\lambda_s$ in which λ_s is the width of the induced magnetic field at middle intensity obtained from numerical simulations. To determine k_z during the simulations, we performed a Fourier transform of the induced magnetic components. We can define λ_z by $k_z=\pi/\lambda_z$. We can define λ_z by $k_z=\pi/\lambda_z$. For the final state, the mechanism presented here suggests that λ_s and λ_z depend only slightly on the parameters as we noticed in the region of parameter space covered. We used typical estimates: $\lambda_s=0.37$ and $\lambda_z=\pi/0.8$.

4. Applications to Jupiter

In this section, we illustrate this mechanism, motivated by the banded structure observed in Jupiter's atmosphere (Cho and Polvani 1996, Porco *et al.* 2003). In particular, we wish to address the possibility of an origin of these structures in deep layers, where the fluid is electrically conducting (metallic hydrogen), and therefore influenced by the presence of a magnetic field (Yano 1994, Aurnou and Olson 2001, Christensen 2002, Morin and Dormy 2005). Numerical simulations of convection (Heimpel *et al.* 2005) show that the zonal wind resembles the banded structure of Jupiter and Saturn for high enough Rayleigh numbers. However, such a banded

Downloaded by [Observatoire de Paris - Bibliothèque] at 02:42 09 July 2012

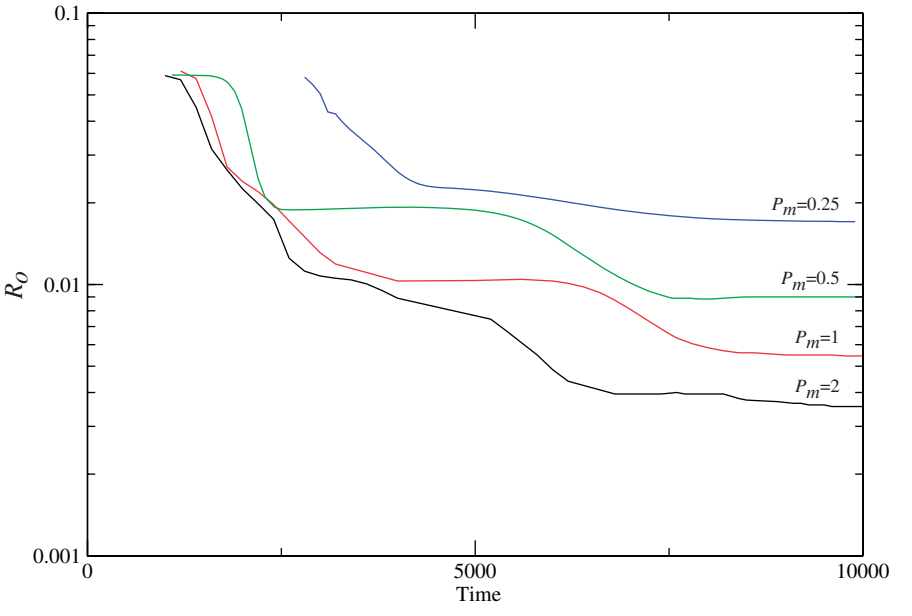

Figure 9. Temporal evolution of the maximum R_o for different P_m. The other parameters are $E = 10^{-5}$, $\Lambda = 1$ and $A = 0.01$.

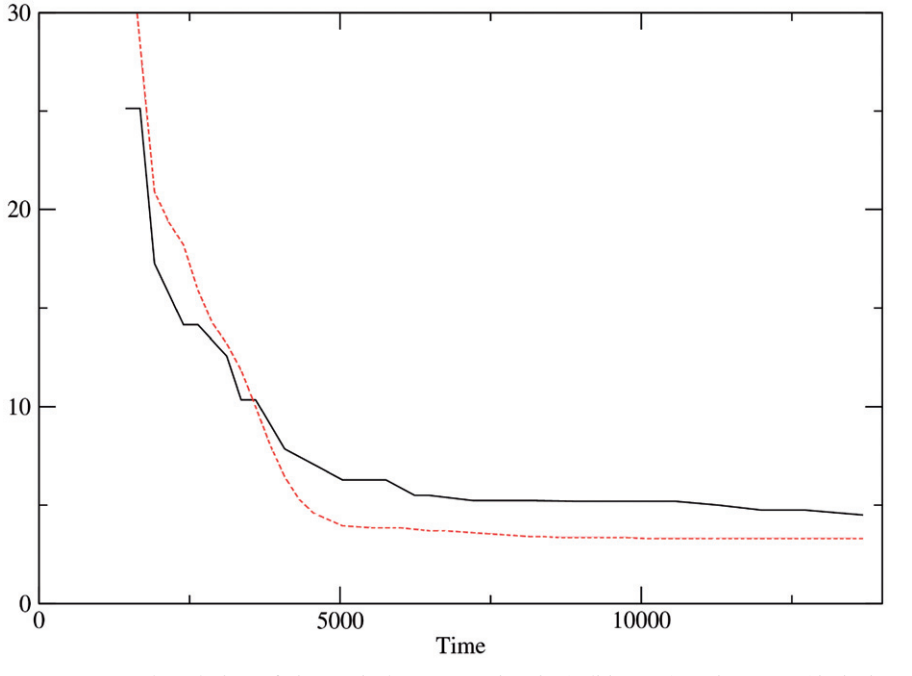

Figure 10. Temporal evolution of the vertical wave number k_z (solid curve) and 250 R_o (dashed curve) for $E = 3 \times 10^{-6}$, $\Lambda = 1$ and $P_m = 1$.

Downloaded by [Observatoire de Paris - Bibliothèque] at 02:42 09 July 2012

Table 1. The maximum R_o for some dimensionless parameters.

E	P_m	Λ	R_o	$R_{o_{th}}$
10^{-5}	2	1	0.0033	0.0026
	1	1	0.0055	0.0052
	0.5	1	0.0090	0.010
	0.25	1	0.0174	0.0205
	0.5	4	0.0023	0.0042
	0.5	10	0.0050	0.0054
3×10^{-6}	1	1	0.0033	0.0016
	0.5	1	0.00325	0.0031
	0.25	1	0.0051	0.0062
	0.5	10	0.0030	0.0016
10^{-6}	0.5	1	0.0012	0.0010

Note: This output parameter corresponds to the maximum shear rate obtained numerically for the final saturated state. $R_{o_{th}}$ is obtained considering marginal stability with $k_z = \pi/0.8$ and $k_s = \pi/0.37$

Downloaded by [Observatoire de Paris - Bibliothèque] at 02:42 09 July 2012

structure in the inner conducting region would be unstable in the presence of vertical magnetic field. Indeed, considering the θ-profile of angular velocity observed in the Jovian atmosphere, and assuming a geostrophic structure ($\Omega_{\mathrm{Jup}} = \Omega_{\mathrm{Jup}}(s) = U_0(s)/s$), linear analysis predicts that all bands are locally unstable when a vertical magnetic field is imposed at sufficiently small Ekman number. Realistic Ekman number can however not be achieved. Instead, we solve the linearised MHD equations with $E = 10^{-6}$ and $\Lambda = 1$, and find that only the band closest to the atmosphere is MS-MRI unstable with a growth rate of $\sigma = 0.0052$. Decreasing the Ekman number to $E = 5 \times 10^{-7}$, destabilises all bands.

In the nonlinear regime, the bands are progressively suppressed (figure 11). The forced velocity field used for this simulation has the form $U_0(s) = s\Omega_{\mathrm{Jup}}(s)$. The boundary conditions and the initial conditions are unchanged. The simulation has been terminated only at $t = 1500$ when saturation initially sets in. The profile has been modified within a very short time period. In this context, the MS-MRI could provide a new constraint on the flow. This would suggest that the observed Jovian-banded structure cannot be maintained in the conducting zone, because it would then be unstable to the MS-MRI. This result suggests that either the origin of the banded structure is not deep, or convection is powerful enough to maintain the profile against this destabilising process. In the latter case, the system remains unstable, and the MS-MRI could then play an important role in the dynamo process. As mentioned in PDB08, this role could be to induce rapid variations of the global magnetic field.

5. Summary and discussion

We have studied the MS-MRI occurring in the spherical Couette flow (section 2) and in simulations with an imposed geostrophic shear profile (section 3). The initially most unstable mode saturates by limiting the magnitude of the shear geostrophically (figure 7), whereas the induced magnetic field is just stretched radially (figure 8). In the simulations with the spherical Couette flow, the conducting inner core plays a crucial role by introducing a vertical shear. The angular velocity profile tends to reach a

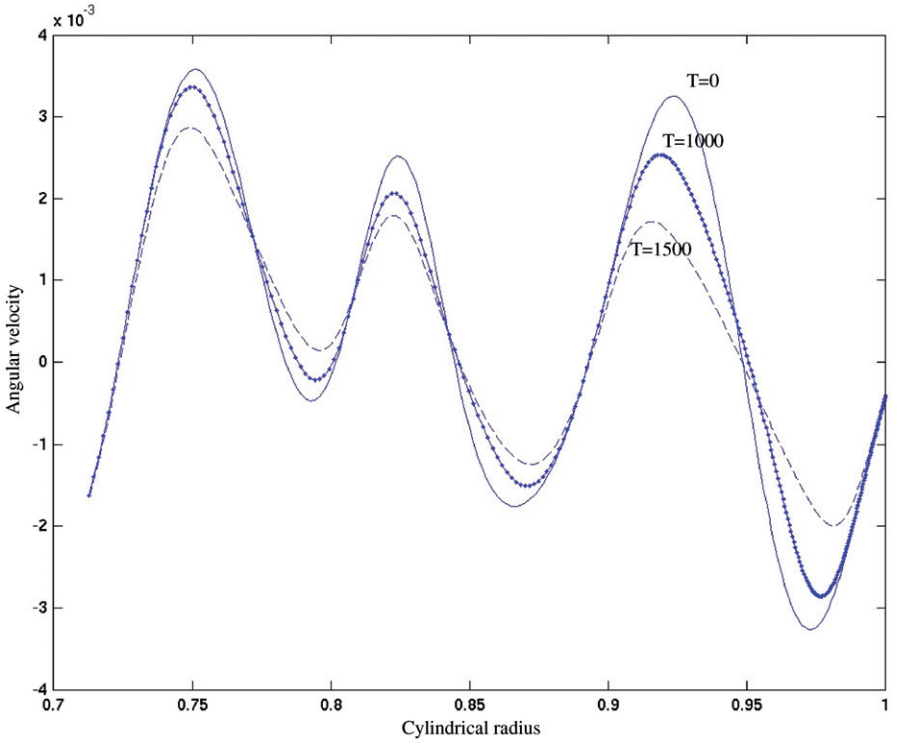

Figure 11. Evolution of the angular velocity profile with time. At $t=0$, the profile is obtained from observations of the Jovian atmosphere. The parameters for this simulation are $E=5\times10^{-7}$, $P_m=0.5$ and $\Lambda=1$.

stationary state in which Ω is not z-independent and it decreases smoothly from the inner core to the outer shell boundary. For an imposed shear profile as given by equation (5), unstable modes with smaller and smaller k_z develop as the simulations are advanced in time. These secondary instabilities have the same character as the primary, and they saturate by further decreasing the maximum radial shear (as measured by R_o). The final stationary state appears to be marginally stable (table 1). The final state is reached within a short timescale compared to viscous or magnetic diffusion times. Following these arguments, the MS-MRI could be an important feedback mechanism, limiting the maximum magnitude of the shear in natural dynamos.

The theoretical work on the saturation of the MRI done by Knobloch and Julien (2005) is not applicable to Keplerian accretion disks. These authors mention that the MRI saturates by compensating the background shear whereas in accretion disks, the rotation profile is forced and maintained by the massive central object. But in our simulations, the nonlinear effects can offset the imposed profile. Knobloch and Julien (2005) use the assumptions $\Omega_0 L \gg v_A$, $R_o\Omega_0 L \gg v_A$ and $R_m = R_o\Omega_0 L/\eta \gg S = v_A L/\eta \gg 1$, in which S is the Lundquist number and R_m is the magnetic Reynolds number. At the beginning of our simulations, these inequalities are satisfied, but, when R_o decreases by one order of magnitude, they are not longer valid. From a geophysical point of view, it could be interesting to carry out their theoretical analysis in the small R_o regime.

Downloaded by [Observatoire de Paris - Bibliothèque] at 02:42 09 July 2012

Although the MS-MRI is probably not responsible for the dynamo action in planetary interiors, it may affect the way in which this process takes place by limiting the maximum amplitude of the shear. Numerical simulations often have rather large radial shear, but if the chosen parameters do not allow for the MS-MRI on interesting time scales, the results inferred may be misleading. Care must be taken to note the distinction between parameter regimes relevant to planetary interiors and those that are numerically achievable, which are often not influenced by the MS-MRI.

Downloaded by [Observatoire de Paris - Bibliothèque] at 02:42 09 July 2012

Acknowledgements

I wish to thank Steven Balbus and Emmanuel Dormy for useful discussions and comments on this work and Martin Schrinner for his help in improving earlier versions of this manuscript. I also wish to thank ''LRA-ENS'' (laboratoire de Radioastronomie de l'Ecole Normale Superieure) for access to the CEMAG parallel computer.

References

Aurnou, J. and Olson, P., Strong zonal winds from thermal convection in a rotating spherical shell. *Geophys. Res. Lett*. 2001, **28**, 2557–2559.

Balbus, S.A. and Hawley, J.F., A powerful local shear instability in weakly magnetized disks. *Astrophys. J*. 1991, **376**, 214–222.

Balbus, S.A. and Hawley, J.F., Instability, turbulence, and enhanced transport in accretion disks. *Rev. Mod. Phys*. 1998, **70**, 1–53.

Brandenburg, A., Nordlund, A., Stein, R.F. and Torkelsson, U., Dynamo-generated turbulence and large-scale magnetic fields in a Kepierian shear flow. *Astrophys. J*. 1995, **446**, 741.

Chandrasekhar, S., *Hydrodynamic and Hydromagnetic Stability*, 1961 (Oxford: Oxford University Press).

Cho, J.Y.K. and Povalni, L.M., The morphogenesis of bands and zonal winds in the atmospheres on the giant outer planets. *Science* 1996, **273**, 335.

Christensen, U., Zonal flow driven by strongly supercritical convection in rotating spherical shells. *J. Fluid Mech*. 2002, **470**, 115–133.

Dormy, E., Cardin, P. and Jault, D., MHD flow in a slightly differentially rotating spherical shell, with conducting inner core in a dipolar magnetic field. *Earth Planet. Sci. Lett*. 1998, **160**, 15–30.

Hawley, J.F., Gammie, C.F. and Balbus, S.A., Local three-dimensional magnetohydrodynamic simulations of accretion disks. *Astrophys. J*. 1995, **440**, 742–763.

Hawley, J.F., Gammie, C.F. and Balbus, S.A., Local three-dimensional simulations of an accretion disk, hydromagnetic dynamo. *Astrophys. J*. 1996, **464**, 690–703.

Heimpel, M., Aurnou, J. and Wicht, J., Simulation of equatorial and high-latitude jets on Jupiter in a deep convection model. *Nature* 2005, **438**, 193–196.

Knobloch, E. and Julien, K., Saturation of the magnetorotational instability. *Phys. Fluid* 2005, **17**, 094106.

Matsumoto, R., Uchida, Y., Hirose, S., Shibata, K., Hayashi, M.R., Ferrari, A., Bodo, G. and Norman, C., Radio jets and the formation of active galaxies: avalanches on the torus by the effect of a large scale magnetic field. *Astrophys. J*. 1996, **461**, 115.

Morin, V. and Dormy, E., Dissipation mechanisms for convection in rapidly rotating spheres and the formation of banded structures. *Phys. Fluid* 2006, **18**, 068104.

Petitdemange, L., Dormy, E. and Balbus, S.A., MagnetoStrophic MRI in the Earth's outer core. *Geophys. Res. Lett*. 2008, **35**, 15305.

Porco, C.C., West, R.A., McEwen, A., *et al*., Cassini imaging of Jupiter's atmosphere, satellites, and rings. *Science* 2003, **299**, 1541–1547.

Proudman, I., The almost-rigid rotation of viscous fluid between concentric spheres. *J. Fluid Mech*. 1956, **1**, 505–516.

Stewartson, K., On almost rigid rotation: Part 2. *J. Fluid Mech*. 1966, **26**, 131–144.

Velikhov, E.P., Stability of an ideally conducting liquid flowing between cylinders rotating in a magnetic field. *Sov. Phys. JETP* 1959, **36**, 1398–1404 (p. 995 in English translation).

Yano, J.-I., A critical review on the dynamics of Jovian atmospheres. *Chaos* 1994, **4**, 287–297.